In situ electrical and mechanical study of Indium Tin Oxide films deposited on polyimide substrate by Xe ion beam sputtering

T. Chommaux, P.O. Renault, D. Thiaudière, P. Godard, F. Paumier, T. Girardeau, S. Hurand, Ph. Goudeau

In situ electrical and mechanical study of Indium Tin Oxide films deposited on polyimide substrate by Xe ion beam sputtering

T. Chommaux[1,2], P.O. Renault[1*], D. Thiaudière[2], P. Godard[1], F. Paumier[1], T. Girardeau[1], S. Hurand[1], Ph. Goudeau[1]

[1] Institut Pprime, CNRS – Université de Poitiers, 86073 Poitiers cedex, France

[2] Synchrotron SOLEIL, L'orme des merisiers Saint Aubin, 91192 Gif-sur-Yvette, France

Abstract: Four series of Indium Tin Oxide (ITO) thin films 600 nm thick were deposited on polyimide substrates by Xe ion beam sputtering under different deposition conditions: with or without O_2 flow, and at room temperature or 100°C heated substrates. Both electrical and mechanical properties of the four different films were investigated in situ by electrical resistance measurements and synchrotron x-ray diffraction during equibiaxial deformation tests. The ITO films are found to have a low elastically anisotropy, i.e. an elastic anisotropy index slightly smaller than 1. The elastic regime domain is quite small and is associated to a small effective negative gauge factor. During biaxial straining, electrical measurements show that all films are very brittle with crack onset strains corresponding to applied strains ranging from 0.15 to 0.3%. The introduction of oxygen flow during deposition delays the crack onset as the decrease of deposition temperature does.

Corresponding author: pierre.olivier.renault@univ-poitiers.fr

Keywords: *In situ* deformation; Synchrotron x-ray diffraction; Electrical properties; Mechanical properties; Indium tin oxide; Thin films; Elastic anisotropy

1. Introduction

Indium tin oxides (ITO) have been used as transparent conductive electrodes in many different optoelectronic devices because of the very good combination of high optical transmittance in the visible range and low electrical resistivity. The combination of optical and electrical properties of ITO can be understood in detail from free electron theory [1]. For most of the current applications, ITO films are deposited on rigid substrates but deposition of ITO films on stretchable and foldable polymeric supports is desired for many new applications. Polymeric substrates indeed present the advantages of light weight, low cost, mechanical stretchability and bendability.

Deposition of thin films onto flexible substrates obviously introduces risks of cracking and accompanying loss of electrical conductivity. Many types of mechanical deformation tests are used to study film failure. The two most commons are the uniaxial tensile test [2-4] and the bending test [5-6]. In situ microscopy (optical, Scanning Electron Microscopy,…) can be performed to track crack onset and monitor the density of cracks [2, 7-8]. According to literature, the fracture behaviour is dependent on film thickness [9-10], film adhesion, substrate and film elastic moduli [11, 12], film architecture [13], deformation mode [14] among other things. Several groups [2-4] have investigated the mechanical properties of ITO films on polymer substrates focusing on the cracking mechanisms and the effect on electrical properties. A recent study of Kim et al. demonstrates that the degree of crystallinity and crystalline quality are certainly the primary factors for determining the mechanical strength of ITO on polymer substrates [15].

The present experimental study focuses on the effect of the elaboration process of ITO films on the electrical and mechanical properties. Four point electrical resistance and synchrotron

x-ray diffraction (XRD) measurements were performed in situ during biaxial loading-unloading of ITO films – Polyimide composites. In particular, we investigate the differences induced by changing the temperature of elaboration, and the O_2 gas flow during ITO deposition by Xe ion beam sputtering on polyimide substrate. The magnitude of biaxial applied deformation imposed to ITO films is small (less than 1%) so that the onset of cracking can be investigated in depth. Up to a tensile deformation of about 0.3% (corresponding to the elastic domain limit), XRD data show no significant difference between the four samples and reveal the slight anisotropic elastic mechanical behaviour of ITO. Moreover, in the elastic domain, results demonstrate that the electrical resistance is decreasing as the ITO films elongate. This feature reveals a negative effective strain gauge associated with piezoresistive properties. For larger applied strains, the film failure attributed to crack formation is captured first by the electrical measurements prior to strain measurements by x-ray diffraction during mechanical testing. The resistance versus true strain curves plotted for the four ITO films reveal the crack onset strain differences related to the different deposition conditions and exhibit a hysteresis that is induced by a significant closure of cracks during unloading.

2. Experimental

2.1 Sample elaboration and as-deposited characterization

Four series of ITO thin films were prepared by ion beam sputtering on polyimide substrates. A ceramic target of In_2O_3/SnO_2 (90:10) was used. Fig.1 presents a schematic illustration of the deposition chamber (Nordiko 2000 system). Crystallinity of ITO which is a critical physical parameter for physical properties is obviously strongly dependent of physical vapor deposition conditions. Here, the target to substrate distance is 55 cm. When the pressure had

been reduced to about $7x10^{-5}$ Pa, prior to deposition, the ITO ceramic target was presputtered according to a procedure divided into three steps of 10 min each (consisting of increasing the Xe beam current step by step) in order to increase slowly the temperature of target and to remove surface impurities. The deposits of ITO films 600 nm thick are performed with a Xe+ ion gun sputtering beam at 1.2 keV at a working pressure of approximately 10^{-4} Pa with and without introduction of small quantity of oxygen (O_2 flow at 5 sccm). The optional O_2 reactive gas is inserted to the deposition chamber through a second ion gun without acceleration voltage (Fig.1). For another set of samples, the substrate was raised up to a temperature of 100°C for 1 hour. Then the temperature was maintained at 100° C during deposition. Let us notice that the substrate temperature has been monitored during a deposition test; for a setpoint temperature of 100°C, the actual temperature measured at the surface of polyimide substrate increases up to about 80°C and remains roughly constant during the deposit which lasts for about 40 minutes. Deposition parameters (temperature and oxygen flow) are listed in Table 1. Growth rate measurement of 0.15 nm/s was performed by determining the film thickness using ex situ x-ray reflectometry measurement. The polyimide (PI) substrates 125 µm thick (Kapton HN®) have a cruciform shape with arms of 200 mm long and 20 mm wide (Fig. 2). The ITO deposition onto PI is performed through a circular mask of 20 mm diameter that is positioned at the centre of PI cruciform shape sample. Interestingly, even if surface activation by ion-assisted reactions can be useful for improving the adherence of a transparent conductive oxide film to a polymer substrate [16], no specific surface treatment nor adhesion layer has been used in the present work, and the adhesion is very good though, as will be shown in subsection 3.2.

The electrical properties were characterized by Hall effect measurements in a HMS 5500 setup. These measurements that were carried under direct current (d.c.) condition probe the

mobility of free carrier on macroscopic scale including therefore all scattering mechanisms. All the reported measurements were done at room temperature and room pressure. The magnetic field was provided by a permanent magnet of intensity B=0.58 Tesla. We prepared and tested several square-shaped PI samples, which were elaborated at the same time as cruciform PI specimens for in situ tensile tests. In some cases, we repeated the measurement several times in order to check for reproducibility, and found variations of about 2% for resistance, and of 7% for mobility and concentration.

2.2 Tensile loading with in situ resistance and x-ray diffraction measurements

We have employed the DIFFABS-SOLEIL biaxial tensile tester working in the synchrotron environment for *in situ* diffraction measurements of thin crystalline films mechanical response [17]. The cruciform substrates were gripped by a cam rotating in a cylindrical fixation. The equibiaxial loading - unloading of the cruciform sample was controlled by displacement of the grips in the x and y axes where x and y correspond to the in-plane reference frame (z is the out of plane axis) related to the branches of the cruciform substrate (Fig. 2). The displacement grip speed corresponds to a deformation rate at the centre of about $2x10^{-6}$ s^{-1}. The in-plane macroscopic strains (ε_{xx} and ε_{yy}) of the polyimide substrate were measured by Digital Image Correlation (DIC) [18, 19] at the centre of the cruciform shape substrate by using images of about 6 x 9 mm^2.

The incident x-ray beam was monochromatized using a double-crystal monochromator to a wavelength of λ = 0.06888 nm (i.e., an energy of 18 keV). The x-ray beam was of 295 x 260 μm^2 in size (horizontal and vertical full width at half maximum, FWHM, respectively). A hybrid pixel area detector (XPAD detector) [20] was used at a sample-to-detector distance of 621 mm. This XPAD 2D detector contains 240 x 560 pixels,

with a pixel size of 130 x 130 µm². At this distance, the 2θ angular acceptance covers 7.3°. This set-up enables the measurement of a diffractogram every 4 seconds during a continuous loading. Thanks to a homemade python code, the raw data were re-calculated to get usual 2θ angles. Initial diffractograms are shown in Fig. 3 for the four different samples. The diffractograms show two diffraction peaks related to ITO films and two diffraction peaks related to TiO_2 powder (rutile phase); these latter allow performing calibration and correction of sample vertical movement during loading tests. It is indeed important to distinguish various causes producing diffraction peak shifts from strain variations. For an incident ω angle fixed at 7°, the ITO(222) and ITO(400) Bragg peaks, associated with 2theta angles of about 13.4° and 15.5° probe planes almost parallel to the surface, i.e. the out-of-plane elastic strain ε_{zz}.

Concerning electrical resistance measurements, four electrical contacts are made at the periphery of circular ITO films with silver paste, and thin copper wires were used as connecting leads to the electrometers. During continuous loading – unloading, a constant current (I= 1 mA) from a current source (Keithley 6221 programmable current source) was allowed to pass through two terminal leads (A and B) of the four-point probe, and the voltage (V) across the two other leads (C and D) was measured using a multimeter (Keithley 2182 nanovoltmeter) (Fig. 2). Automated data acquisition was achieved thanks to a home-made LabVIEW program.

3. Results and discussion

3.1 Electrical properties and microstructure of the as-deposited ITO films

Typical x-ray diffraction profiles acquired during in situ tensile tests are shown in Fig. 3 for the four selected deposition conditions. All profiles indicated the presence of a single

crystallographic cubic phase of In_2O_3 bixbyite and can be compared with referenced phase of the JCPDS database #6-0416. The presence of a given amount of amorphous phase of ITO reported by Legeay and Castex [21] is not excluded, the related hump being impossible to decorrelate here from the high background signal due to PI substrate scattering. The amount of TiO_2 powder that is sprayed on the PI backside is not the same for the four samples while the ITO film thicknesses are similar. Hence, the intensities of TiO_2 diffraction peaks cannot be compared from one sample to another. On the other hand, since the films have the same thickness, the integrated intensities of ITO films could be quantitatively related to the diffraction volume and hence to the amount of crystallinity if no crystallographic texture was present. However, preferential grain orientation between the samples elaborated with O_2 flow or without can be observed. For samples without O_2 flow, the relative ratios of {004}/{222} integrated intensities are relatively close to the one of JCPDS database while the samples with O_2 flow show a {004} excess (Table 2). Interestingly, if the deposition temperature does not change the crystallographic texture for films elaborated without O_2 flow, it induces opposite behaviours for the degree of crystallinity. As expected, the increase of substrate temperature induces an increase of degree of crystallinity for samples deposited without O_2 flow while it is the opposite for samples deposited with O_2 flow. At low substrate temperatures (RT), the mobility of atoms at the surface growing film surface is very low due to limited diffusion during the film formation. This can lead to amorphous structure of ITO. But in the present case of sputtering technique, there is a significant energy transfer due to the high energy of particles (ions and neutrals) impinging into the film [22] which can explain the nucleation of crystallite of ITO at RT. Following the same reasoning, this should also be the case for the samples elaborated with O_2 flow. But, in the latter case, the degree of crystallinity at 100°C is more than two times smaller than the one at RT. The two sets of samples have different crystallographic texture that clearly depends on the O_2 flow.

Noteworthy, the relative ratios of {004}/{222} integrated intensities are constant versus temperature and hence texture can be considered as similar for samples elaborated at RT and 100°C for samples deposited without O_2 flow. On the contrary, the crystallographic texture changes with temperature for samples deposited with O_2 flow (Table 2). Song et al. have reported that the <001> texture is caused by high energy ion bombardment of the growing film surface [23], but, as the working pressure is the same in our case, the energy of ion bombardment should be similar if the influence of the target-substrate distance is neglected. For sputtering at 200°C and at higher oxygen flow, the <111> orientation was dominant while the <100> orientation was mainly built up at lower oxygen pressure [24]. On the contrary we observed that the increase of oxygen flow favoured the <100> orientation. This could be due to the fact that the main parameter is the sputtering pressure that does not change in our deposition procedure and is about two orders of magnitude lower than the one of Song et al. [23]. This result implies that the main parameter of texture growth in Betz et al. [24] could be the sputtering pressure rather than the oxygen flow. Moreover, crystallinity of ITO is not improved with increase in oxygen flow contrary to the observation of Song et al. [23]. This inconsistency is certainly due to the influence of several deposition parameters that are not in the same range, namely O_2 pressure, working pressure, target-substrate distance among others. They argued that enough oxygen supplement should be needed to form stoichiometric films and this could favour crystallization. Our observations may suggest that O_2 molecules adsorbed on the growing film surface could result in suppressing the surface migration of In atoms during the crystal growth and hence increasing the structural disorder in growing films.

Electrical characteristics of the four selected as-deposited ITO films obtained from Hall measurements are listed in Table 1 and presented in Fig. 4. We notice first that as-deposited

ITO films have a high negative carrier concentration ($\sim 10^{21}$ cm^{-3}). The ITO films with O_2 flow were found to have seven times smaller carrier concentration. This phenomenon can be attributed to free carriers that are provided from two different kinds of electron donor sites: substitutional doping of Sn on In sites in the In_2O_3 crystal structure and divalent oxygen vacancies [1, 25, 26]. The densities of oxygen vacancies in the bixbyite crystal structure and of the crystallographic defects are likely to reduce the conductivity through a substantial decrease of mobility [26]. In another study, an increase of the conductivity of five orders of magnitude has been reported upon thermal annealing [27]. The main objective of the thermal treatment was to increase the crystallinity of ITO films, but the authors observed a high-temperature out-diffusion of interstitial oxygen. Hence the thermal annealing induced a decrease of resistivity that could be explained by a reduced number of traps and increased mobility. In the present study, the resistivity was found to be around 1 x 10^{-3} Ω cm, a lowest value of 7.2 x 10^{-4} Ω cm was achieved for Xe sputtered ITO film at 100°C (Xe_100°C). The mobility increases with O_2 flow and temperature from about 1.4 for Xe at RT (Xe_RT) to achieve only 10 $cm^2.V^{-1}.s^{-1}$ for Xe+O_2 sputtered ITO film at 100°C (Xe+O_2_100°C). ITO films sputtered at higher temperature show an increase of their mobility while the carrier concentrations remain similar (or slightly decrease). As a result, ITO films deposited at higher temperature show a lower resistivity that is only related to the larger mobility. These observations are qualitatively consistent with the observations of Hamouda et al. for Xe magnetron sputtering [28]. But a lower resistivity can also be induced by creation of oxygen vacancies that increases electron carrier density. In sputtered ITO films, these oxygen vacancies can be controlled by post-annealing treatment or different sputtering conditions [1,15,16,21,23-32] among which the impact of the ion energy bombardment [30] or the reduction reaction of hydrogen radicals [29]. In the present study, the introduction of oxygen

flow during sputtering increases resistivity by about a factor of two by greatly decreasing carrier density (by a factor of seven) while increasing mobility (by a factor of three to four).

To sum up, the four selected deposition conditions made it possible to fabricate four ITO films on polyimide substrates with different microstructure and electrical properties. The four samples are polycrystalline (with single bixbyite phase) certainly with a given amount of amorphous ITO phase that has not been quantified. The samples elaborated without oxygen exhibit no significant preferential orientation while the samples prepared with O_2 flow show a slight <001> texture that increases with deposition temperature (Table 2). The full widths at half maximum that reflect the sizes of the crystallites and the strain heterogeneities, reveal that adding the oxygen flow induces better crystallinity but the integrated intensities reveal that the total amount of crystallized ITO is lower. This observation can also be correlated with the increase of electrical carrier mobility that is significantly improved when adding the oxygen flow. Moreover, samples with (resp. without) O_2 flow are transparent (resp. opaque); the residual stress states that have been estimated by the Stoney method on ITO films deposited on silicon single crystals during the same deposition run are -250 MPa +/- 70 MPa for Xe_RT and Xe_100°C, -550 MPa +/- 100 MPa for Xe+O2_RT and -400 +/- 100 MPa for Xe+O2_100°C. All the films are in a compressive stress state explained by the high energetic deposition process. The deposition temperature is not high enough to induce a significant thermal stress contribution.

3.2 Evolution of mechanical and electrical properties of ITO films during in situ deformation tests

As mentioned in the introduction, the main objective of this study is to investigate the mechanical properties as a function of the microstructure. Figs. 5 present a typical set of in

situ data acquired during the loading-unloading tests (namely DIC and XRD measured strains and electrical resistance); here is the example of the ITO film elaborated without O_2 flow at 100°C (Xe_100°C). The mechanical deformation test lasts for about one hour. The initial loading of 17N for the cruciform ITO-polyimide samples that ensures a stable position of sample during loading is used as a reference state for all parameters: macroscopic strains, elastic XRD strains, and electrical resistance. This initial loading corresponds to an equibiaxial tensile strain of 0.12% that can be related to an applied tensile biaxial stress of 215 MPa (with a Young's modulus E=116 GPa and a Poisson's ratio ν=0.35 [33]).

Firstly, the macroscopic or true strain measurements ($\varepsilon_{XX}^{DIC}$and ε_{YY}^{DIC} components) show the anisotropic behaviour of Kapton® substrates that leads to a non-perfect equibiaxial deformation test. During loading, the applied true strains increased linearly with time up to about 0.7%. Once unloaded, the applied true strain components are equal to approximately 0.1%. In other words, the unloaded strain state is different from the initial one while the loading force is going back to the initial value. This residual strain at the centre of the substrate is due to the geometry of the cruciform shape substrate. Indeed, if the maximum applied strain of about 0.7% that is measured at the centre of the cruciform shape substrate is lower than the yield strain of polyimide, the strains of the sample are much larger than that in the toe weld region. So, considering the distribution of strains in the whole sample, the deformation test can be over the yield point in some regions and this is why the applied strain at the center of the cruciform shape substrate is not going back to zero when the sample is unloaded (see Fig. 5a).

Secondly, the elastic strains, or in other words the lattice strains deduced from the two ITO(222) and ITO(400) diffraction peaks as a function of time are shown in Figs. 5. Due to the measurement configuration, these strains are related to diffracting planes parallel to the

sample surface; the measured strain values are then negative due to Poisson's effect. Indeed, an in-plane elongation of the film induces a contraction in the out of plane or perpendicular direction. The two curves corresponding to the two diffracting planes are strikingly very well superimposed. This result demonstrates that the ITO film Xe_100°C is elastically perfectly isotropic, i.e. exhibits an elastic anisotropy index, defined for cubic material as $A=2c_{44}/(c_{11}-c_{12})$, equals to 1. This is indeed an interesting finding of the presented results: the ITO films shows anisotropic index equal to 0.95+/-0.05. The literature related to elastic properties of ITO is very scarce. From a residual stress analysis study on {004} and {222} diffraction peaks of ITO films, Veith et al. reported a 10% difference in values of residual stresses analysed from {004} and {222} diffraction peaks of ITO films [34]; this difference can be attributed to an elastic anisotropy of ITO with [100] direction of ITO slightly stiffer than the [111] direction. This observation is qualitatively and quantitatively in agreement with our result. From Brillouin scattering, Wittkowski et al. also reported that their ITO films were elastically anisotropic [35]. More recently, by combining the frequency signatures of the vibrational modes of ITO nanorods with finite-element simulations, Guo et al. determined the three elastic constants for single-crystalline cubic ITO, which were 277.5, 107, and 33.8 GPa, for c_{11}, c_{12}, and c_{44} respectively [36]. These values lead to a strong elastic anisotropy with a Zener anisotropy index of 0.39. This value corroborates qualitatively the fact that the [400] direction is stiffer than the [222] direction as observed by Veith et al. [34] and ourselves; but the anisotropy of 0.39 is far too high, and does not reflect quantitatively our results.

Another important feature of the change of elastic strains as a function of time is the departure from linearity at ε_{ZZ}^{XRD}= - 0.35% which is shown in Fig. 5a at t~1200 s and, even more clearly in Fig. 6 for the two samples that have been submitted to larger applied strains, i.e. Xe+O2_RT and Xe_100°C. For these two latter samples, the loading part can indeed be

clearly separated into two domains: elastic domain and crack domain. As the applied macroscopic strain is continuously increasing, the change of XRD strain slopes can be related to crack propagation in brittle films [13]. Indeed, when a failure occurs in the ITO thin film, stress is relaxed locally and transferred to the substrate. This phenomenon leads to a decrease in the average stress supported by the film that is captured by x-ray diffraction. In the first domain that is related to the elastic domain, the elastic strains measured in ITO crystalline part can be compared to DIC macroscopic strains of substrate. Using Hooke's law $\varepsilon_{zz} = \frac{-\nu}{(1-\nu)}(\varepsilon_{xx} + \varepsilon_{yy})$ and ν=0.35 we obtained values that are similar to ε_{ZZ}^{XRD}meaning that the strain is transmitted unchanged through the film-substrate interface. As mentioned in section 2.1, the ion beam sputtering technique at the low working pressure produces high energetic ions and neutrals impinging on the film; these deposition conditions allow to create highly dense films which are very well adherent to the polyimide substrates. Noteworthy, no delamination occurs when the ITO-Polyimide composite was bent or even folded.

Thirdly, Figs. 5 also present the electrical resistance evolution versus time. Fig. 5b (which is a zoom of Fig. 5a) helps to uncover the negative slope of relative resistance evolution ΔR/R which is hidden by the large magnitude of ΔR/R. The relative electrical resistance has to be plotted on a different scale (on the right axis) as the relative evolution is quite huge compared to the applied strain: 250% versus 0.7%. This huge increase of resistance is related to crack nucleation and propagation [2]. The relative resistance that is drastically decreasing during unloading reveals a partial closure of cracks. This typical electrical resistance behaviour of thin films on polymeric substrates has been reported many times for uniaxial tensile tests [2-4, 37, 38] or bending tests [39, 40]. The difference in mechanical properties between ITO films and polyimide substrate is an issue, and tensile deformation may lead to crack patterns and thereby increased resistivity [2, 3]. As expected, electrical resistance measurements are

more sensitive than XRD measurements to capture the crack onset. Indeed, as soon as there is one crack or a few microcracks, the electrical flow is modified and hence induces substantial increase of the film electrical resistance. The advantage of this in-situ electrical probe technique is that the exact crack onset can be determined for brittle films [41]. On the contrary, a sufficient density of cracks is required before the stress relaxation can be captured by XRD measurements as clearly shown in Fig. 6. Monitoring of the changes in slopes can give information about processes occurring in the ITO film. As expected, the curves superimposed on each other rather well in the first domain related to the elastic regime. Then for brittle films such as ITO, the changes of slope as applied deformation increases reveal the relaxation of strain related to cracks. The crack features are well captured for Xe_100°C and Xe+O_2_RT samples at applied deformation of about 0.36% and 0.42% respectively. During unloading, the slopes of these last two samples are different from the slopes in the elastic regime. This behaviour reveals the process of stress redistribution in the film-substrate composite. At the beginning of unloading, the relaxation of the applied load starts in the softer material, namely the polymer substrate, and hence is not captured by XRD measurements. Then at the end of unloading, the slopes become again similar to the one at the beginning because of crack closure. All these deformation processes are confirmed by electrical measurements. Fig. 7 focuses on the early stages of the tensile deformation; this figure highlights both the negative slope of relative resistance evolution versus tensile strain, and the departure from linearity that reveals the crack onset strain. The electrical resistance increases sharply at some critical strain which depends on film deposition conditions. The resistance increase is indeed explained by the appearance of the cracks. For the four samples, the crack onset strain is at very small applied strains, ranging from 0.1% up to 0.3%. These small strain values reveal the brittleness of our ITO films that is much lower than the crack onset reported by many authors. Their films failed under applied uniaxial tensile strains

typically in the range 0.8-1.2% [6], 1.59% [4] 1.4-2.2% [2], or even 2.5-3% [3]. Alike brittle materials, the cracking properties of ITO strongly depend on the layer thickness, crystallinity, interface quality, density of defect or roughness [2-6, 40]. Among these parameters, only the microstructure (crystallite size, amount of crystallinity, crystallographic texture) changes between the four samples. Independently of these microstructural considerations, Fig. 7 shows that the introduction of O_2 during deposition seems to delay the crack onset strain as the decrease of deposition temperature does. This observation cannot be directly correlated to the amount of crystallisation due to crystallographic texture changes. We can however notice that the crack onset strain is at about 0.12% for Xe_100°C versus 0.24% for Xe_RT as the amount of crystallinity increases with temperature. This last result is indeed associated to an integrated intensity that increased by a factor of 2.5 and to a similar crystallographic texture (similar integrated area ratios of {400} and {222} diffraction peaks). Hence, the brittleness increases as the crystallinity increases contrary to the observations reported by different groups [40, 42]. The other interesting point of Fig. 7 is that it revealed the piezoresistive nature of the four ITO films. The influence of strain on electrical properties of ITO has been reported and can be exploited in the fabrication of strain gauges [43]. If the samples were only submitted to geometrical deformation (without piezoresistivity nor defect nucleation), the electrical measurement should mainly reveal the thickness change with a perfect four point probe method as underlined by the dashed line. All ITO films show a negative effective strain gauge factor of about -2 (Table 3). If such negative piezoresistive responses have already been reported [43, 44], most of the time no change of resistance is reported as a function of deformation in the elastic domain. Our gauge factors agree reasonably well with the values reported by Fang et al. [44]. These authors observed that the oxygen pressure during ITO film deposition affects the resistivity and gauge factor. They measured gauge

factors of about -0.5 or -1 for ITO films deposited at low oxygen pressure (around 10 Pa), and these films show a resistivity of ~10^4 Ω cm that is similar to the one of our films.

4. Conclusions

We report in situ mechanical and electrical properties evolution of ITO sputtered films during an equibiaxial loading-unloading cycle. The effect of deposition parameters on in situ mechanical and electrical properties of 600 nm thick ITO films deposited on polyimide substrates was investigated. Four different microstructures were fabricated by changing deposition parameters including oxygen flow and deposition temperature. The resistivity was found to be around 1 x 10^{-3} Ω cm, a lowest value of 7.24 x 10^{-4} Ω cm was achieved for Xe sputtered ITO film at 100°C. During loading, development of microcracks generated by mechanical stress in ITO is evidenced by a substantial increase of film electrical resistance at very small applied deformations. The introduction of O_2 flow during deposition delays the crack onset strain as the decrease of temperature does from an applied equibiaxial strain of 0.15% up to 0.3%. In the elastic domain, in situ XRD tensile tests allow demonstrating that the ITO polycrystalline films exhibit a very low elastic anisotropy as observed by Veith et al. [34] and contrary to what has been recently reported in literature by Guo et al. [36]. For all Xe sputtered ITO films, the Zener elastic anisotropy index was estimated to be 0.95+/-0.05. In addition, a negative effective gauge factor of about -2 was measured for all ITO films.

Acknowledgements

This work partially pertains to the French Government program “investissements d’avenir” (LABEX INTERACTIFS, reference ANR-11-LABX-0017-01) and (EUR INTREE, reference ANR-18-EURE-0010). The region Nouvelle-Aquitaine and the French synchrotron SOLEIL via the NACRES project supported this work.

List of references:

[1] I. Hamberg, C.G. Granqvist, Evaporated Sn-doped In2O3 films – basic optical-properties and applications to energy-efficient windows, J. Appl. Phys. 60 (1986) R123-R159, https://doi.org/10.1063/1.337534

[2] Y. Leterrier, L. Médico, F. Demarco, J.A.E. Manson, U. Betz, M.F. Escola, M. Kharrazi Olsson, F. Atamny, Mechanical integrity of transparent conductive oxide films for flexible polymer-based displays, Thin Solid Films 460 (2004) 156-166, https://doi.org/10.1016/j.tsf.2004.01.052

[3] D.R. Cairns, R.P. Witte II, D.K. Sparacin, S.M. Sachsman, D.C. Paine, G.P. Crawford, R.R. Newton, Strain-dependent electrical resistance of tin-doped indium oxide on polymer substrates, Appl. Phys. Lett. 76 (2000) 1425, https://doi.org/10.1063/1.126052

[4] C. Peng, Z. Jia, D. Bianculli, T. Li, and J. Lou, In situ electro-mechanical experiments and mechanics modelling of tensile cracking in indium tin oxide thin films on polyimide substrates, J. Appl. Phys. 109 (2011) 103530, https://doi.org/10.1063/1.3592341

[5] Z. Suo, E.Y. Ma, H. Gleshkova, and S. Wagner, Mechanics of rollable and foldable film-on-foil electronics, Appl. Phys. Lett. 74 (1999) 1117, https://doi.org/10.1063/1.123478

[6] S.K. Park, J.I. Han, D.G. Moon, W.K. Kim, Mechanical stability of externally deformed Indium-Tin-Oxide Films on polymer substrates, Jpn. J. Appl. Phys. 42 (2003) 623-629, https://doi.org/10.1143/JJAP.42.623

[7] R.M. Souza, M. Ignat, C.E. Pinedo, A.P. Tschiptschin, Structure and properties of low temperature plasma carburized austenitic stainless steels, Surf. Coat. Technol. 204 (2009) 1102-1105, https://doi.org/10.1016/j.surfcoat.2009.04.033

[8] V.M. Marx, F. Toth, A. Wiesinger, J. Berger, C. Kirchlechner, M.J. Cordill, F.D. Fischer, F.G. Rammerstorfer, G. Dehm, The influence of a brittle Cr interlayer on the

deformation behavior of thin Cu films on flexible substrates: Experiment and model, Acta Mater. 89 (2015) 278–289, https://doi.org/10.1016/j.actamat.2015.01.047

[9] Y. Leterrier, J. Andersons, Y. Pitton, J.A.E. Manson, Adhesion of silicon oxide layers on poly(ethylene terephthalate), J. Polym. Sci. B-Polym. Phys.35 (1997) 1463-1472, https://doi.org/10.1002/(SICI)1099-0488(19970715)35:9<1463::AID-POLB16>3.0.CO;2-4

[10] B.C. Mohanty, H.R. Choi, Y.M. Choi, Y.S. Cho, Thickness-dependent fracture behavior of flexible ZnO:Al thin films, J. Phys. D: Appl. Phys., 44 (2011) 025401, https://doi.org/10.1088/0022-3727/44/2/025401

[11] J.L. Beuth, Cracking of thin bonded films in residual tension, Int. J. Solids Struct. 29 (1992) 1657-1675, https://doi.org/10.1016/0020-7683(92)90015-L

[12] J.W. Hutchinson, Z. Suo, Mixed-Mode Cracking in layered materials, Adv. Appl. Mech. 29 (1992) 63- 191 , https://doi.org/10.1016/s0065-2156(08)70164-9

[13] M.J. Cordill, P. Kreiml, B. Putz, C. Mitterer, D. Thiaudière, C. Mocuta, P.-O. Renault, D. Faurie, Role of layer order on the equi-biaxial behavior of Al/Mo bilayers, Scr. Mater. 194 (2021) 113656

[14] D.Faurie, F.Zighem, P.Godard, G.Parry, T.Sadat, D.Thiaudière, P.-O.Renault, In situ x-ray diffraction analysis of 2D crack patterning in thin films, Acta Mater. 165 (2019) 177-182, https://doi.org/10.1016/j.actamat.2018.11.040

[15] E.H. Kim, C.W. Yang, J.W. Park, The crystallinity and mechanical properties of indium tin oxide coatings on polymer substrates, J. Appl. Phys. 109 (2011) 043511, https://doi.org/10.1063/1.3556452

[16] J.S. Cho, S. Han, K.H. Kim, Y.W. Beag, S.K. Koh, Surface modification of polymers by ion-assisted reaction, Thin Solid Films, 445 (2003) 332-341, https://doi.org/10.1016/S0040-6090(03)01176-3

[17] G. Geandier, D. Thiaudière, R.N. Randriamazaoro et al., Development of a synchrotron biaxial tensile device for in situ characterization of thin films mechanical response, Rev. Sci. Instr. 81(2010) 103903, https://doi.org/10.1063/1.3488628

[18] G. Besnard, F. Hild, S. Roux, 'Finite-element' displacement fields analysis from digital images : application to Portevin-Le Châtelier bands, Exp. Mech. 46, 789 (2006) 789-804, https://doi.org/10.1007/s11340-006-9824-8

[19] S. Djaziri, P.O. Renault, F. Hild, E. Le Bourhis, P. Goudeau, D. Thiaudière and D. Faurie, Combined synchrotron X-ray and image-correlation analyses of biaxially deformed W/Cu nanocomposite thin films on Kapton, J. Appl. Cryst. 44 (2011) 1071-1079, https://doi.org/10.1107/S0021889811030226

[20] P. Pangaud, S. Basolo, N. Boudet, J.-F. Berar, B. Chantepie, J.-C. Clemens, P. Delpierre, B. Dinkespiler, K. Medjoubi, S. Hustache, M.Menounia C. Morel, XPAD3-S: A fast hybrid pixel readout chip for X-ray synchrotron facilities, Nucl. Instrum. Methods Phys. Res., Sect. A 591(2008) 159-162 , https://doi.org/10.1016/j.nima.2008.03.047

[21] G. Legeay and X. Castel, A gradual annealing of amorphous sputtered indium tin oxide: Crystalline structure and electrical characteristics, Thin Solid Films 520 (2012) 4021-4025, https://doi.org/10.1016/j.tsf.2012.01.029

[22] J.A. Thornton, The microstructure of sputter-deposited coatings, J. Vac. Sci. & Tech. A 4 (1986) 3059-3065, https://doi.org/10.1116/1.573628

[23] P.K. Song, Y. Shigesato, I. Yasui, C.W. Ow-Yang, D.C. Paine, Study on crystallinity of tin-doped indium oxide films deposited by DC magnetron sputtering, Jpn J. Appl. Phys. 37 (1998) 1870-1876, https://doi.org/10.1143/JJAP.37.1870

[24] U. Betz, M. Kharrazi Olsson, J. Marthy, M.F. Escolá, F. Atamny, Thin films engineering of indium tin oxide: Large area flat panel displays application, Surface and Coatings Technol. 200 (2006) 5751-5759, https://doi.org/10.1016/j.surfcoat.2005.08.144

[25] N. Taga, H. Odaka, Y. Shigesato, I. Yasui, M. Kamei, T.E. Haynes, Electrical properties of heteroepitaxial grown tin-doped indium oxide films, J. Appl. Phys., 80 (1996) 978-984, https://doi.org/10.1063/1.362910

[26] J.S. Kim, F. Cacialli, A. Cola, G. Gigli, R. Cingolani, Hall measurements of treated indium tin oxides surfaces, Synthetic Metals 111-112 (2000) 363-367, https://doi.org/ 10.1016/S0379-6779(99)00325-2

[27] L. Bardos, M. Libra, Effect of the oxygen absorption on properties of ITO layers, Vacuum 39 (1989) 33-36, https://doi.org/10.1016/0042-207X(89)90095-X

[28] F. Hamouda, E. Herth, C. David, F. Bayle, M.P. Plante, A. Martin, A. Aassime, Electrical and optical properties of sputtered ultra-thin indium tin oxide films using xenon/argon gas, J. Mater. Sci. Mater. Electron. 30 (2019) 8508-8514, https://doi.org/10.1007/s10854-019-01171-w

[29] S.N. Luo, A. Kono, N. Nouchi, F. Shoji, Effective creation of oxygen vacancies as an electron carrier source in tin-doped indium oxide films by plasma sputtering, J. Appl. Phys. 100 (2006) 113701, https://doi.org/10.1063/1.2372571

[30] D. Vaufrey, M.B. Khalifa, J. Tardy,C. Ghica, M.G. Blanchin,C. Sandu and J. A. Roger, ITO-on-top organic light-emitting devices: a correlated study of opto-electronic and structural characteristics, Semicond. Sci. Technol. 18 (2003) 253-260, https://doi.org/10.1088/0268-1242/18/4/310

[31] Y. Shigesato, D.C. Paine, A microstructural study of low-resistivity tin-doped Indium oxide prepared by dc magnetron sputtering, Thin Solid Films 238 (1994) 44-50, https://doi.org/10.1016/0040-6090(94)90646-7

[32] S.Y. Park, M.J. Kim, P.K. Song, Effects of the cathode magnetic field strength on the properties of sputtered ultrathin ITO films, J. Ceram. Process. Res. 16 (2015) 267-271,

[33] D. Neerinck, T. Vink, Depth profiling of thin ITO films by grazing incidence X-ray diffraction, Thin Solid Films 278 (1996) 12–17, https://doi.org/10.1016/0040-6090(95)08117-8

[34] M. Veith, C. Bubel, I. Grobelsek, Investigation of morphological and electrical characteristics of tin doped indium oxide layers produced by a quasi single source precursor system, Thin Solid Films 524 (2012) 67-74, https://doi.org/10.1016/j.tsf.2012.09.063

[35] T. Wittkowski, J. Jorzick, H. Seitz, K. Schröder, B. Jung, K. Hillebrands, Elastic properties of indium tin oxide films, Thin Solid Films 398-399 (2001) 465-470, https://doi.org/10.1016/S0040-6090(01)01373-6

[36] P. Guo, R. D. Schaller, L. E. Ocola, J. B. Ketterson, and R. P. H. Chang, Gigahertz Acoustic Vibrations of Elastically Anisotropic Indium−Tin-Oxide Nanorod Arrays, Nano Lett. 16 (2016) 5639-5646, https://doi.org/10.1021/acs.nanolett.6b02217

[37] Z. Chen, B. Cotterell, W. Wang, The fracture of brittle thin films on compliant substrates in flexible displays, Eng. Fract. Mech 69 (2002) 597-603, https://doi.org/10.1016/S0013-7944(01)00104-7

[38] Saleh, M.N., Lubineau G., Understanding the mechanisms that change the conductivity of damaged ITO-coated polymeric films: a micro-mechanical investigation, Solar Energy Materials and solar cells 130 (2014) 199-207, https://doi.org/10.1016/j.solmat.2014.07.011

[39] Y. Shen, Z. Feng, H. Zhang, Study of indium tin oxide films deposited on colorless polyimide film by magnetron sputtering, Mater. Des. 193 (2020) 108809, https://doi.org/10.1016/j.matdes.2020.108809

[40] J.W. Park, G. Kim, S.H. Lee, E.H. Kim, G.H. Lee, The effect of film microstructures on cracking of transparent conductive oxide (TCO) coatings on polymer substrates, Surf. Coat. Technol. 205 (2010) 915-921, https://doi.org/10.1016/j.surfcoat.2010.08.055

[41] M. J. Cordill, O. Glushko, J. Kreith, V.M. Marx, C. Kirchlechner, Measuring electro-mechanical properties of thin films on polymer substrates, Microelectronic Engineering 137 (2015) 96-100, https://doi.org/10.1016/j.mee.2014.08.002

[42] T. Park, J. Ha, D. Kim, Processing of indium tin oxide thin film to enhance electrical conductivity and flexibility, Thin Solid Films 658 (2018) 38-45, https://doi.org/10.1016/j.tsf.2018.05.031

[43] S.E. Dyer, O.J. Gregory, P.S. Amons, A. Bruins Slot, Preparation and piezoresistive properties of reactively sputtered indium tin oxide thin films, Thin Solid Films 288 (1996) 279-286, https://doi.org/10.1016/S0040-6090(96)08865-7

[44] H. Fang, T. Miller, B.R. Rogers, R.H. Magruder III, R.A. Weller, Effect of oxygen content on piezoresistivity of indium tin oxide thin films prepared by pulsed laser deposition, J. Appl. Phys. 97 (2005) 083502, https://doi.org/10.1063/1.1868062

Tables captions:

Table 1: Hall electrical measurements of the four ITO films as function of the deposition parameters: O_2 flow and substrate deposition temperature. ρ, n and μ are the resistivity, carrier concentration and the mobility, respectively.

Table 2: X-ray diffraction peak characteristics obtained from fitting: full width at half maximum (FWHM) and integrated intensity (arb.units). The intensity ratio of ITO(400)/ITO(222) given by JCPDS database #6-0416 is 0.3.

Table 3: Strain gauge factor of the four films obtained from the evolution of resistance as a function of applied strains in the elastic regime (slopes of the linear parts of Fig. 6).

Tables:

Sample set	O_2 flow [sccm]	Deposition T° [°C]	ρ [Ω.cm]	n [cm^{-3}]	μ [$cm^2.V^{-1}.s^{-1}$]
Xe_RT	0	20	1.6×10^{-3}	2.8×10^{21}	1.4
Xe_100°C	0	100	7.2×10^{-4}	2.4×10^{21}	3.5
Xe+O_2_RT	5	20	2.6×10^{-3}	3.7×10^{20}	6
Xe+O_2_100°C	5	100	1.9×10^{-3}	3.3×10^{20}	10

Table 1:

Sample set	FWHM (222)	Intensity (222)	FWHM (400)	Intensity (400)	Intensity Ratio (400)/(222)
Xe_RT	0.205	3.8	0.175	2.0	0.5
Xe_100°C	0.155	10.9	0.153	5.2	0.6
$Xe+0_2$_RT	0.081	2.1	0.052	1.7	0.8
$Xe+0_2$_100°C	0.059	0.6	0.053	0.9	1.5

Table 2:

	Xe_RT	Xe_100°C	$Xe+0_2$_RT	$Xe+0_2$_100°C
Effective Gauge factor	-2.0 ± 0.1	-0.7 ± 0.1	-1.7 ± 0.3	-2.6 ± 0.2

Table 3:

List of figures captions:

Figure 1: Schematic of deposition chamber. The ion sputtering beam is composed of Xe. The ITO target – substrate distance is of about 55 cm. Base working pressure is of about 10^{-4} Pa.

Figure 2: Schematic of the cruciform shape substrate specimen. The ITO film is deposited at the centre through a circular mask (diameter of 20 mm). The four electrical contacts are made with silver paste and copper wires.

Figure 3: Typical x-ray diffractograms obtained for the four samples from XPAD detector with a collection time of 4 s. The TiO_2 powder is glued onto the substrate as reference.

Figure 4: Evolution of Hall electrical properties as function of the partial pressure of O_2 (O_2 flow), and substrate deposition temperature (RT open symbol and T=100°C full symbol).

Figure 5: In situ XRD strain obtained from ITO (222) and (400) diffraction peaks, true strain obtained from DIC technique, and electrical resistance measurements data versus time a) whole tensile test showing loading-unloading b) magnification of the first stages of loading. Example on the sample elaborated without O_2 flow at 100°C.

Figure 6: XRD strains of the ITO (222) diffraction peak measured versus macroscopic applied strains measured by DIC. Monitoring of the changes in slopes can give information about processes occurring in the film. Two regimes during loading: 1-elastic regime, 2-cracks propagation, and two regimes during unloading: 3-redistribution of applied load mainly in substrate because of crack closure, 4- most of the cracks are closed.

Figure 7: Relative resistance measurements versus macroscopic applied strains. Only the beginning of the loading is shown to clearly identify the departure from linearity (related to crack onset strain) and the negative slope (related to piezoresistivity of ITO).

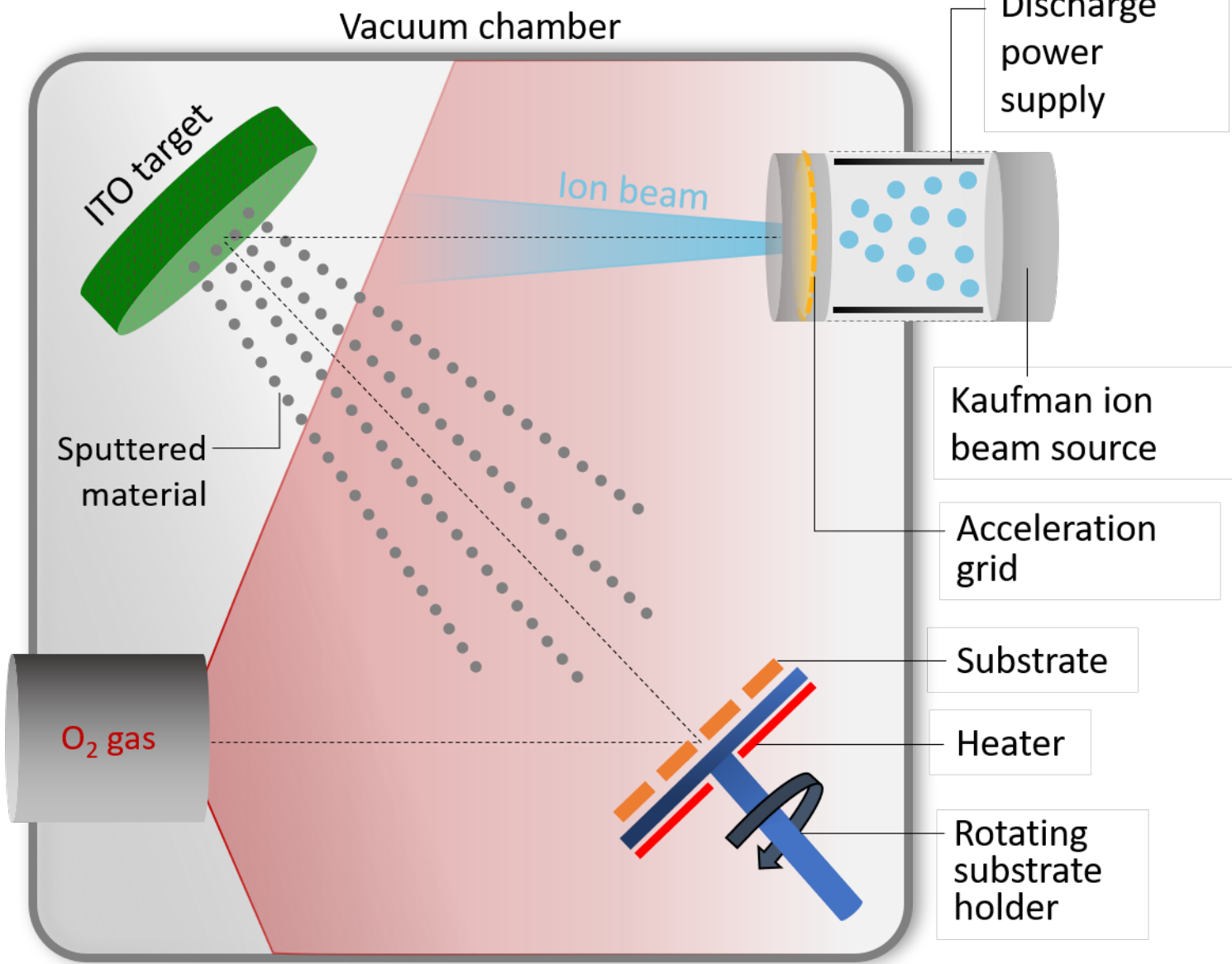
Vacuum chamber
Discharge power supply
ITO target
Ion beam
Sputtered material
Kaufman ion beam source
Acceleration grid
Substrate
O_2 gas
Heater
Rotating substrate holder

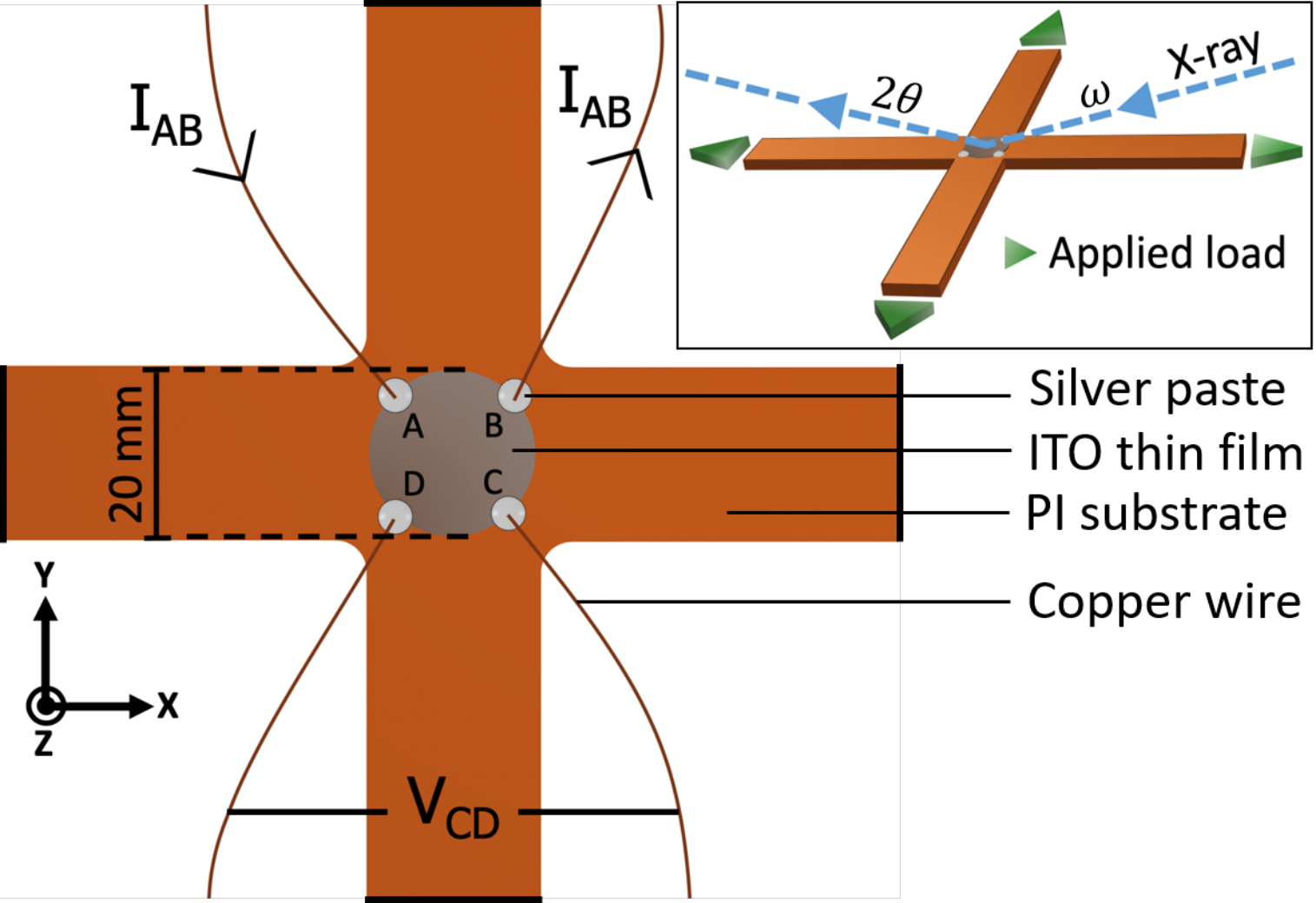
I_{AB}
I_{AB}
20 mm
A
B
D
C
Y
X
Z
V_{CD}
2θ
ω
X-ray
Applied load
Silver paste
ITO thin film
PI substrate
Copper wire

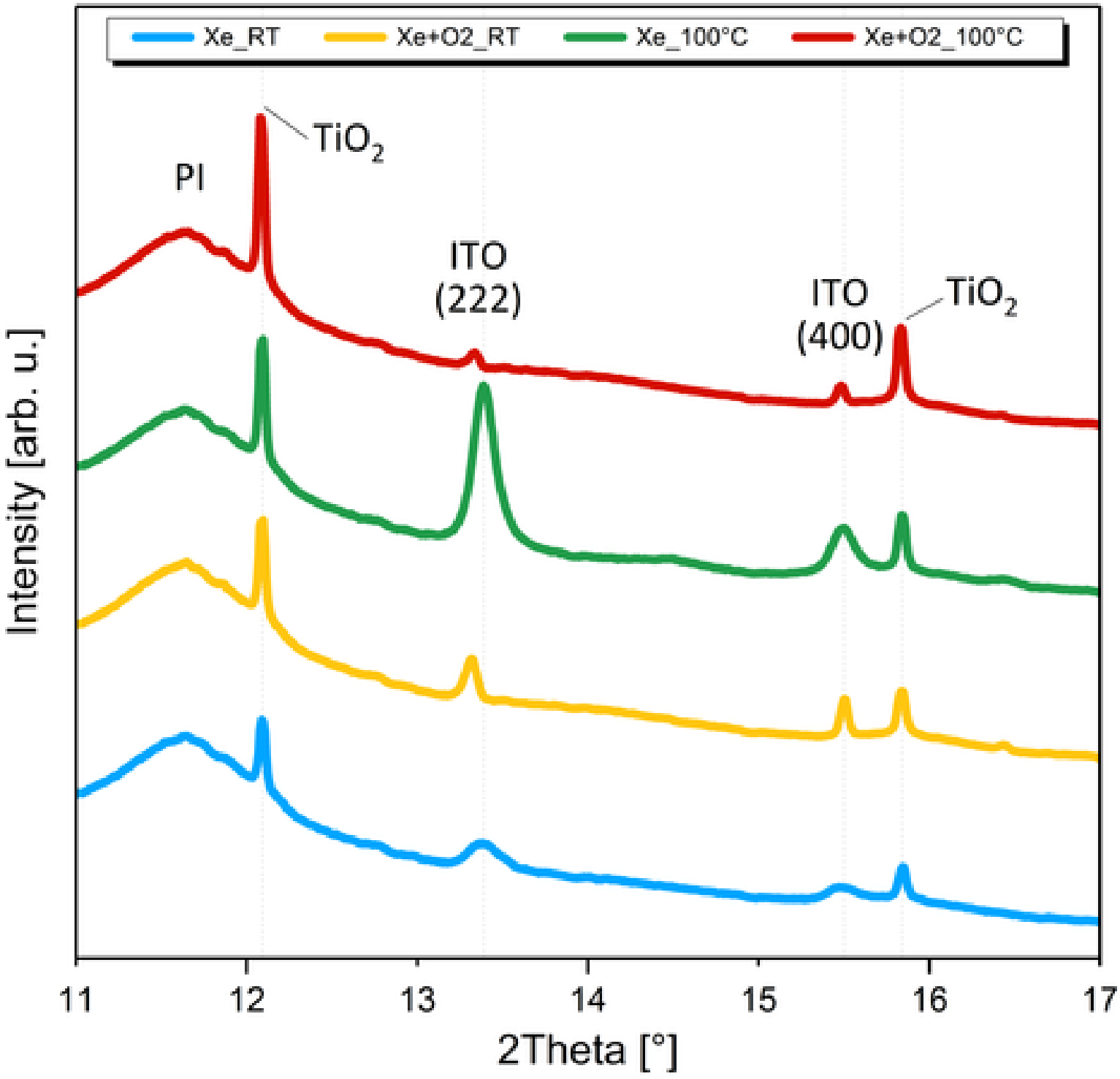
Xe_RT
Xe+O2_RT
Xe_100°C
Xe+O2_100°C
PI
TiO2
ITO
(222)
ITO
(400)
TiO2
Intensity [arb. u.]
11
12
13
14
15
16
17
2Theta [°]

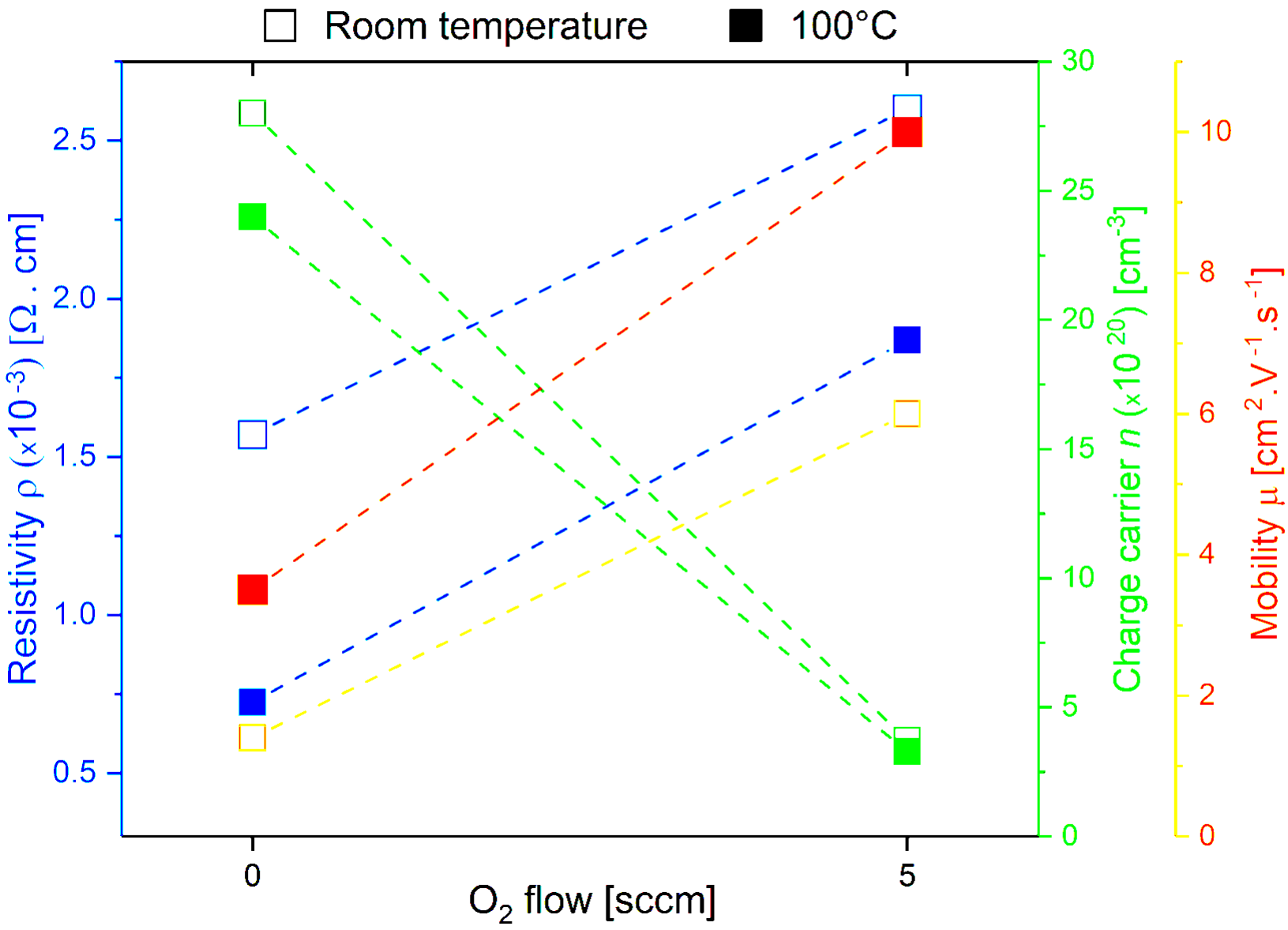
Room temperature
100°C
Resistivity ρ (x10-3) [Ω . cm]
Charge carrier n (x1020) [cm-3]
Mobility μ [cm2.V-1.s-1]
O2 flow [sccm]
0
5
2.5
2.0
1.5
1.0
0.5
30
25
20
15
10
5
0
10
8
6
4
2
0

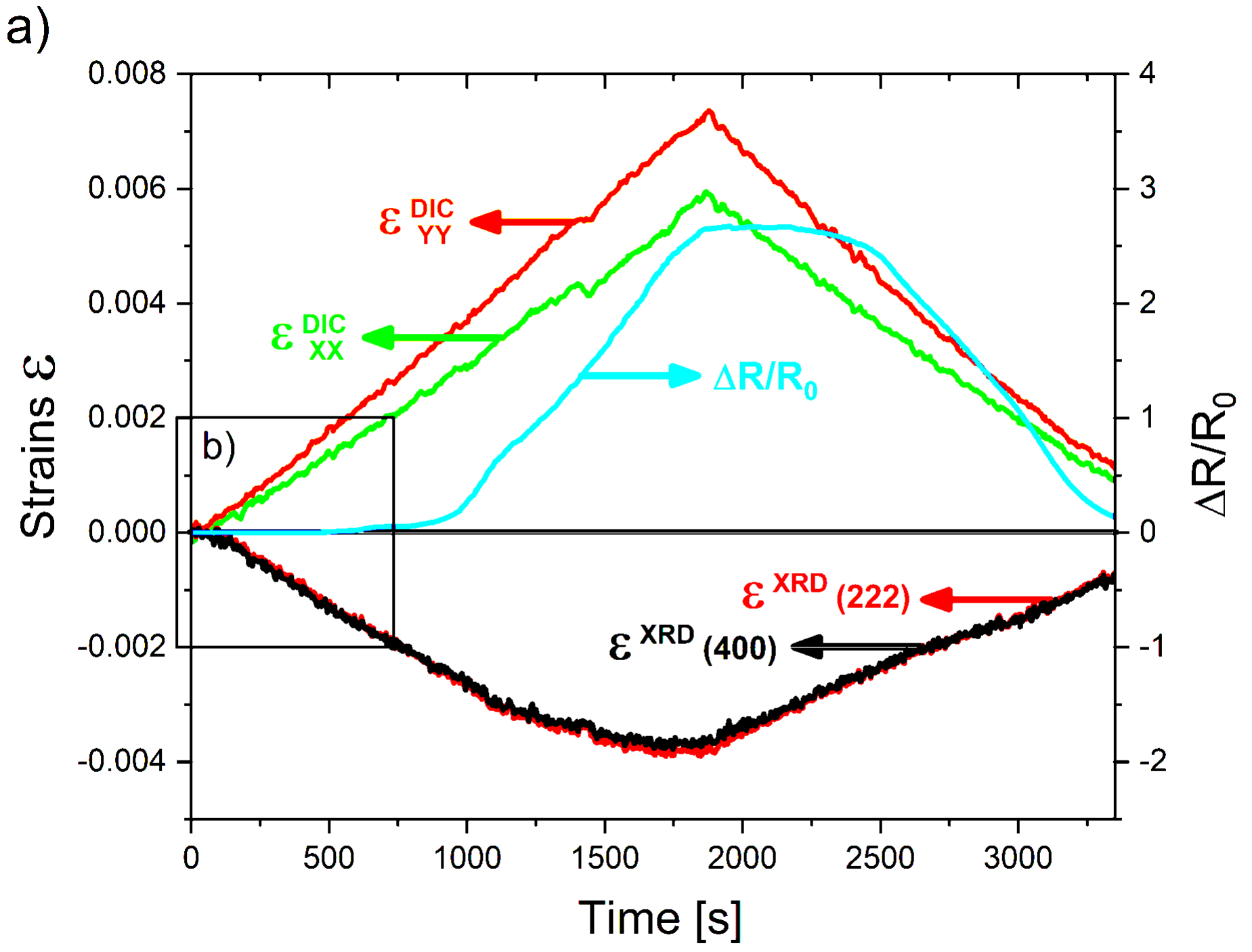
a)
b)
Strains ε
ΔR/R0
Time [s]
ε DIC YY
ε DIC XX
ΔR/R0
ε XRD (222)
ε XRD (400)
0.008
0.006
0.004
0.002
0.000
-0.002
-0.004
4
3
2
1
0
-1
-2
0
500
1000
1500
2000
2500
3000

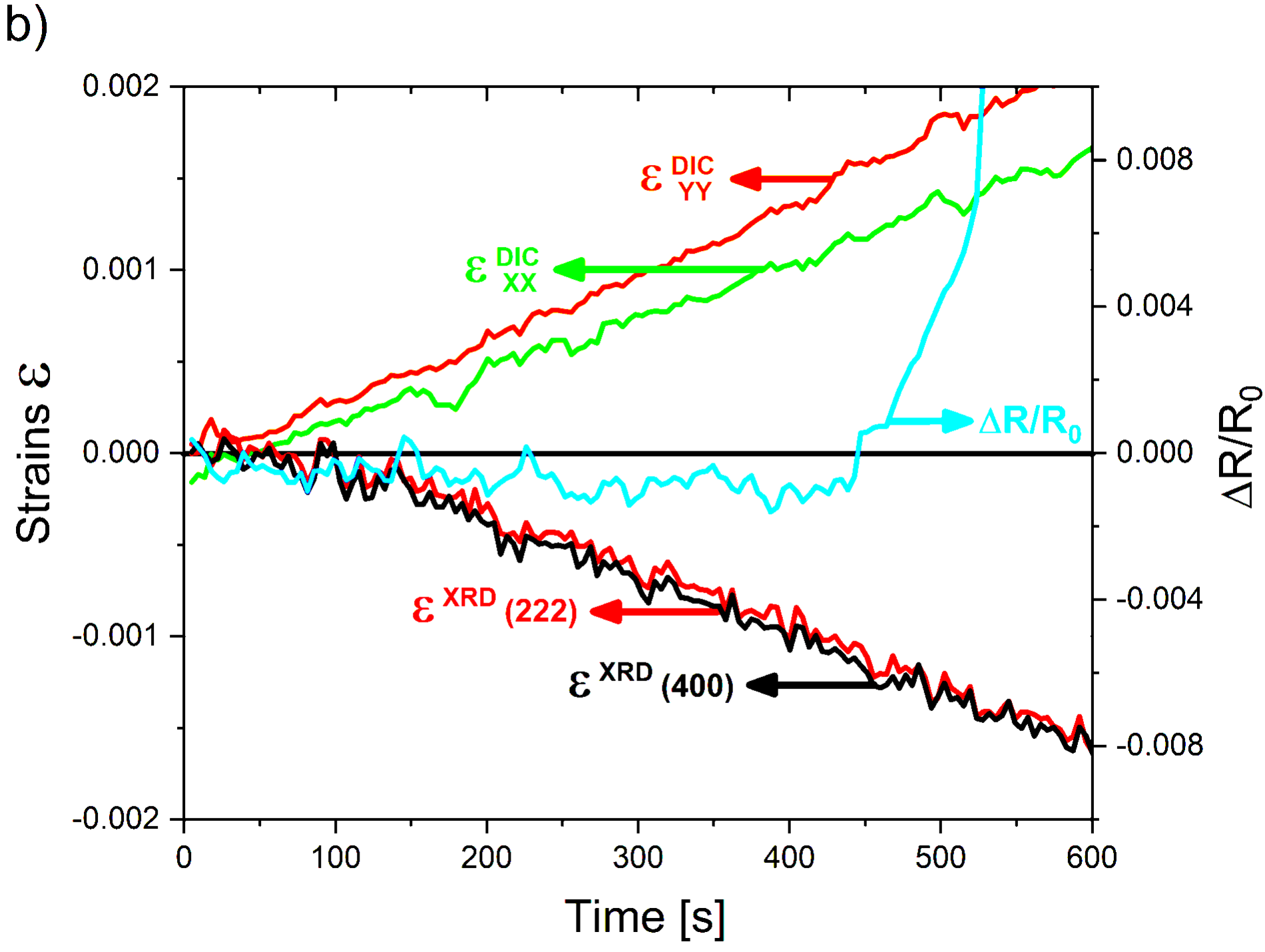
b)
0.002
0.001
0.000
-0.001
-0.002
Strains ε
0
100
200
300
400
500
600
Time [s]
0.008
0.004
0.000
-0.004
-0.008
ΔR/R0
ε DIC YY
ε DIC XX
ΔR/R0
ε XRD (222)
ε XRD (400)

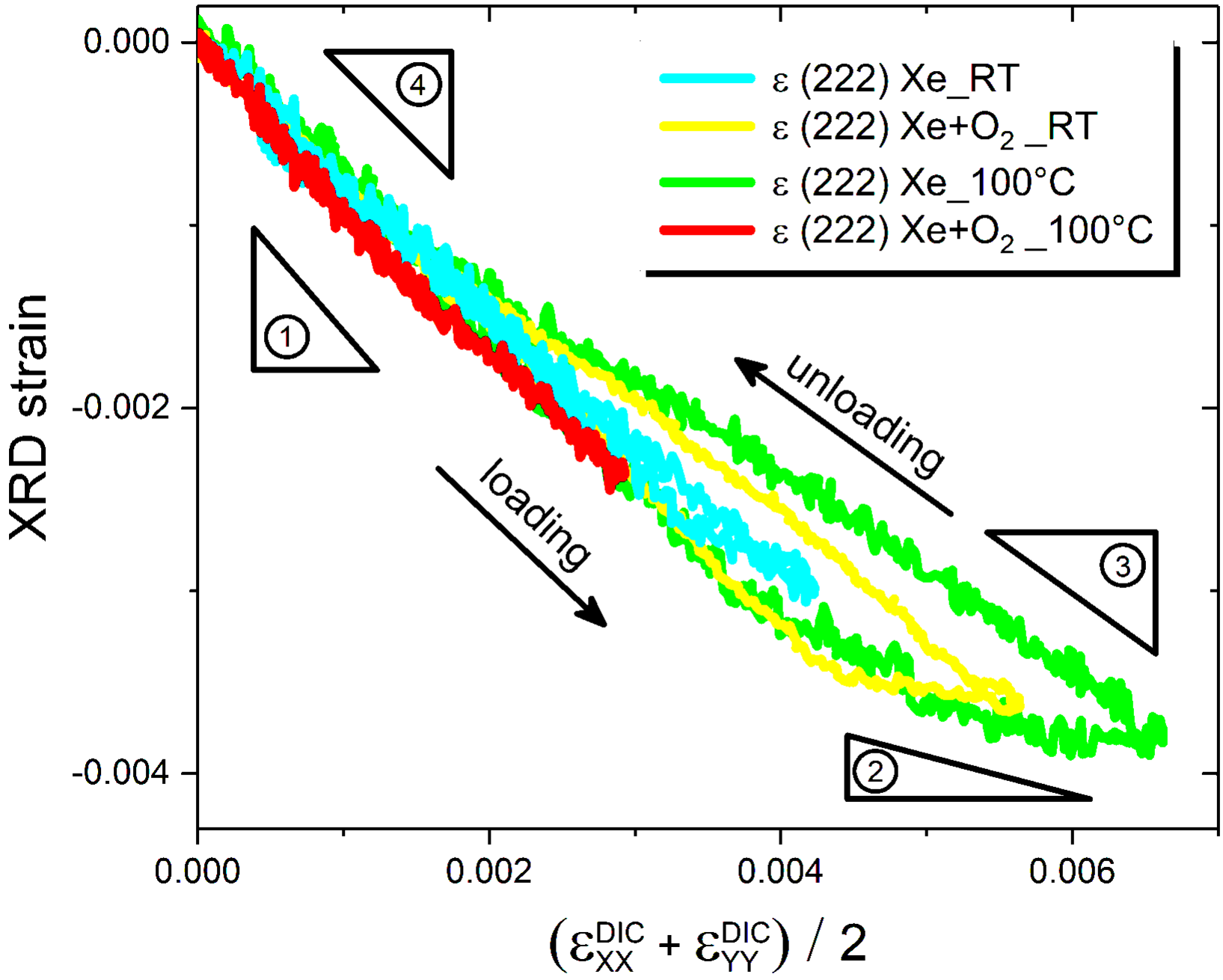
0.000
-0.002
-0.004
XRD strain
0.000
0.002
0.004
0.006
$(\varepsilon_{XX}^{DIC} + \varepsilon_{YY}^{DIC}) / 2$
ε (222) Xe_RT
ε (222) Xe+O2 _RT
ε (222) Xe_100°C
ε (222) Xe+O2 _100°C
loading
unloading
1
2
3
4

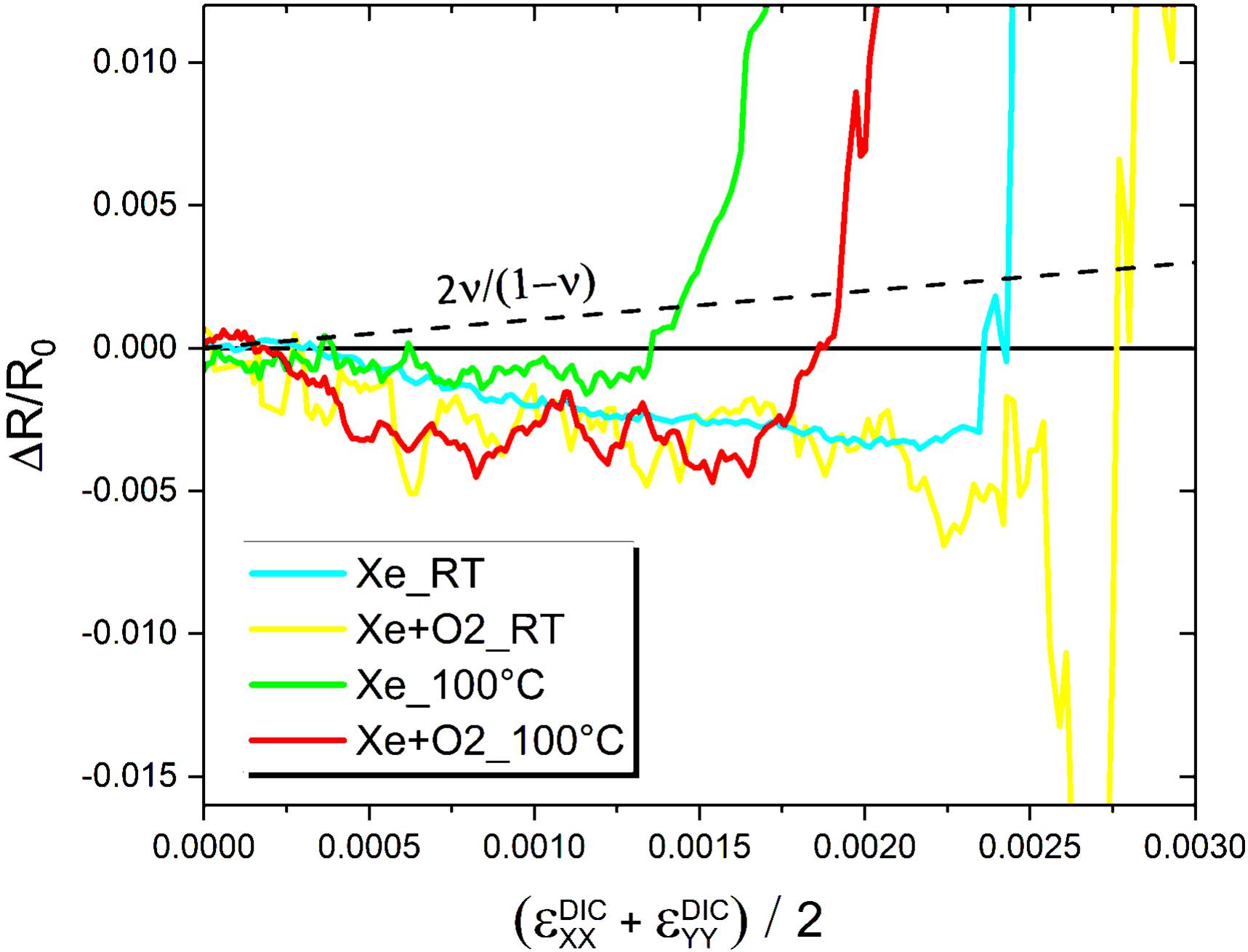
0.010
0.005
0.000
-0.005
-0.010
-0.015
ΔR/R0
2ν/(1−ν)
Xe_RT
Xe+O2_RT
Xe_100°C
Xe+O2_100°C
0.0000
0.0005
0.0010
0.0015
0.0020
0.0025
0.0030
(εXXDIC + εYYDIC) / 2